Institute of Applied Geometry
JKU Linz

# Representing planar domains by polar parameterizations with parabolic parameter lines

S. Trautner, B. Jüttler, Myung-Soo Kim

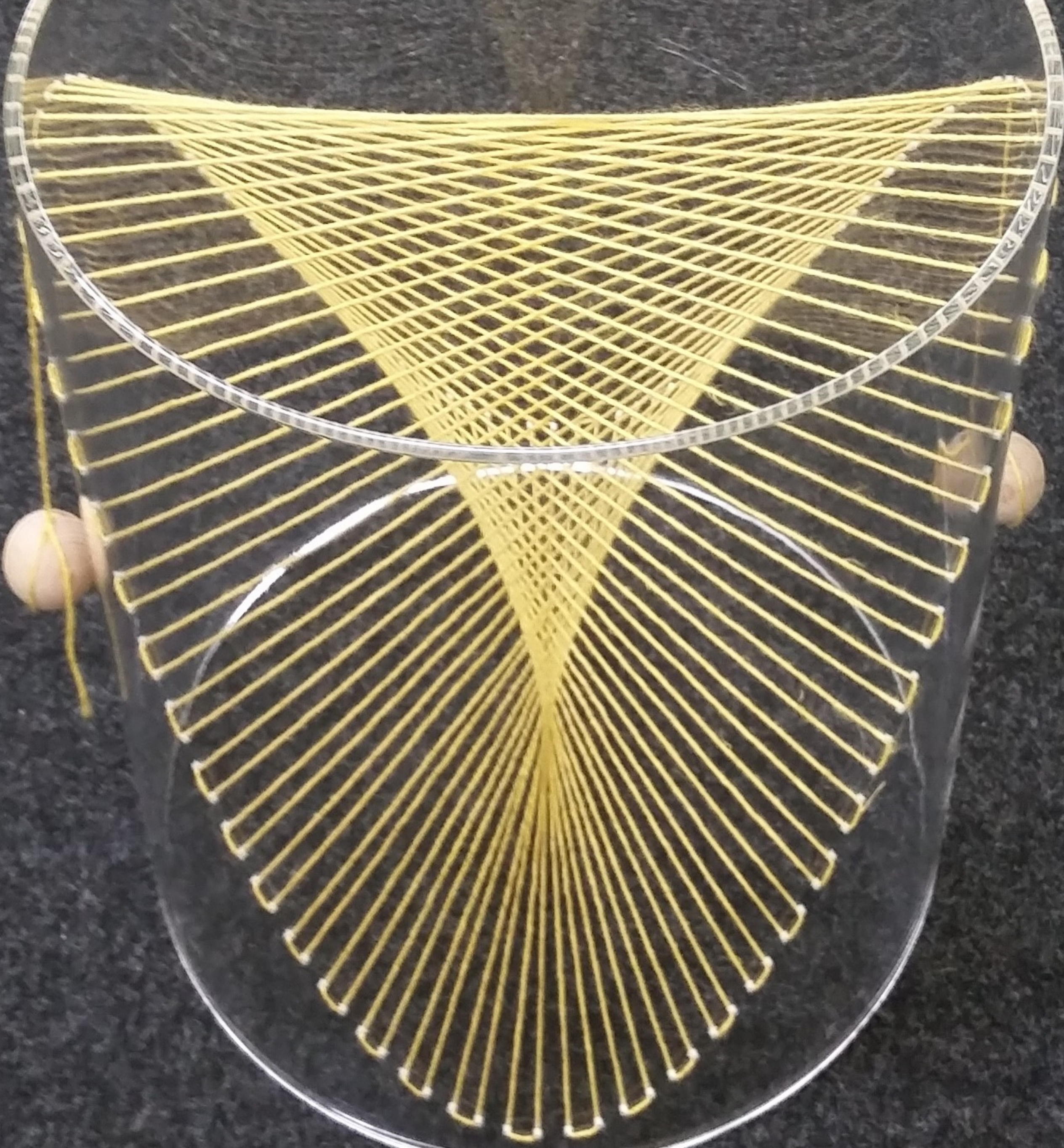

AG Report No. 92
February 23, 2021
www.ag.jku.at

# Representing planar domains by polar parameterizations with parabolic parameter lines

Sofia Trautner[a], Bert Jüttler[a,*], Myung-Soo Kim[b]

[a]Institute of Applied Geometry, Johannes Kepler University, Linz/Austria
[b]School of Computer Science and Engineering, Seoul National University, South Korea

**Abstract**

Polar parameterizations of star-shaped domains are based on the line segments that connect a suitably chosen center point with the points on the domain's boundary. Valid (i.e., regular everywhere except at the center point) polar parameterizations are obtained when choosing a center from the kernel of the domain. Recently, the flexibility of these polar parameterizations has been enhanced by considering so-called arc fibrations (Jüttler et al. 2019), which are polar parameterizations that use circular arcs in order to connect the center with the boundary points. We propose and analyze another generalization of polar parameterizations, which uses parabolic arcs instead of lines or circular arcs. This class of curves is simultaneously simpler (since admitting polynomial parameterizations) and more flexible.

*Keywords:* polar parameterization, arc fibration, parabolic arcs, star-shaped domain

## 1. Introduction

Polar parameterizations of planar domains, which are formed by a system of parameter lines that connects a given center with the points on the boundary, are of recent interest for numerical simulation via the scaled boundary finite element method (Lin et al., 2014; Natarajan et al., 2015; Chen et al., 2016; Arioli et al., 2019) and for domain boundary parameterization in isogeometric analysis (Gondegaon and Voruganti, 2018). While the original formulation of the scaled boundary method relies on star-shaped domains and polar parameterizations by line segments, the generalization to more general systems of parameter lines will greatly increase the geometric flexibility.

Even the simple case of polar parameterizations with linear parameter plays a fundamental role in numerous applications. It leads to the notion of *starshapedness*, which describes the property that a domain possesses at least one center that sees every point on the domain's boundary, and it motivates the definition of the *kernel* of a domain, which is the set of all the feasible center points.

Star-shaped planar polygons were investigated thoroughly in the classical literature on Computational Geometry. The kernel of a planar polygon (i.e., the intersection of all half-planes defined by its edges) can be computed in linear time (Lee and Preparata, 1979), and non-star-shaped polygons can be decomposed efficiently into star-shaped ones (Avis and Toussaint, 1981), even though the problem of finding the minimum decomposition is NP hard (O'Rourke and Supowit, 1983).

Many results from classical computational geometry admit generalizations to domains possessing spline boundary curves (Dobkin and Souvaine, 1990). Visibility locations – which generalize the notion of the center to non-star-shaped domains – have been investigated recently Joshi et al. (2017), extending earlier work on charts for continuous curves in the plane Elber et al. (2005).

Polar parameterizations with circular arcs were investigated recently (Jüttler et al., 2019), in order to obtain polar parameterizations with increased geometric flexibility. It was also noted that the computation

*Email addresses:* sofia.trautner@jku.at (Sofia Trautner[a]), bert.juettler@jku.at (Bert Jüttler[a,*]), mskim@snu.ac.kr (Myung-Soo Kim[b])

of the kernel can be performed efficiently for the case of free-form domains with circular arc spline domains (Weiß and Jüttler, 2019; Weiß, 2019). Moreover, it was shown that the kernel has again an arc spline boundary in this case.

While the generalizations to circular arcs is particularly elegant, it also imposes the need to use *rational* (rather than polynomial) curves, which may be considered as a potential disadvantage (Piegl et al., 2014). In order to avoid this potential difficulty, the present paper analyzes polar parameterizations with parabolic parameter lines. Parabolic arcs are more flexible than circular arcs, which makes this type of parameterizations harder to analyze.

We first introduce a shape parameter $\ell$ in order to reduce the complexity of the problem, and we then derive sufficient conditions for the regularity of polar parameterizations with parabolic parameter lines of a given domain for constant values of that parameter. The extension to a non-constant shape parameter will be discussed as well.

## 2. Polar parameterizations with parabolic parameter lines

We are interested in special parameterizations

$$\mathbf{p}(s,t)\ ,\quad s\in[0,1]\ ,\quad t\in\mathbb{R}\ ,$$

of a simply connected planar domain $D\subset\mathbb{R}^2$. A closed parametric curve

$$\mathbf{c}(t)=(x(t),y(t))\ ,\quad t\in\mathbb{R}\ ,$$

with positive (i.e., counterclockwise) orientation, rotation index +1 for $t\in[0,1]$, and with $C^1$-smooth 1-periodic coordinate functions, i.e. $\mathbf{c}(t)=\mathbf{c}(t+1)$, is used to represent the domain boundary $\partial D$.

It can be assumed without loss of generality that the domain $D$ contains the origin $\mathbf{0}=(0,0)$, which serves as the *center* of the polar parameterization, $\mathbf{p}(0,t)=\mathbf{0}$. The sought-after polar parameterization extends the parametric curve by satisfying $\mathbf{p}(1,t)=\mathbf{c}(t)$ and is 1-periodic with respect to its second argument, $\mathbf{p}(s,t)=\mathbf{p}(s,t+1)$.

Besides parameterizations by lines (which are available for star-shaped domains only) and by circular arcs (Jüttler et al., 2019), the next interesting case is given by considering polar parameterizations with parabolic parameter lines $t=$ constant. More precisely, we consider the special class of polar parameterizations

$$\mathbf{p}(s,t)=(1-s)^2\mathbf{b}_0(t)+2s(1-s)\mathbf{b}_1(t)+s^2\mathbf{b}_2(t)\ , \tag{1}$$

which we construct by using quadratic Bézier curves (i.e., parabolic arcs) for the parameter lines $t=$ constant.

Consider a smooth 1-quasiperiodic function with shift $2\pi$

$$\alpha(t)\in\arg(x(t)+iy(t))^1 \tag{2}$$

that evaluates to the angle of the boundary points. Note that the choice of this function is not unique, since any integer multiple of $2\pi$ may be added. We then consider a smooth function $\varphi(t)$ that fulfills the inequality

$$\alpha(t)-\frac{\pi}{2}<\varphi(t)<\alpha(t)+\frac{\pi}{2} \tag{3}$$

and the functional equation $f(\xi+1)=f(\xi)+2\pi$ that characterizes *arithmetic quasiperiodic functions* with quasiperiod 1 and the constant $2\pi$.

[1] The function $\mathrm{Arg}(x+iy)\in(-\pi,\pi]$ denotes the principal value of the angle between the positive real axis an the vector $x+iy$, while $\arg(x+iy)=\{Arg(x+iy)+2k\pi|k\in\mathbb{Z}\}$ is the set of all possible values of that angle.

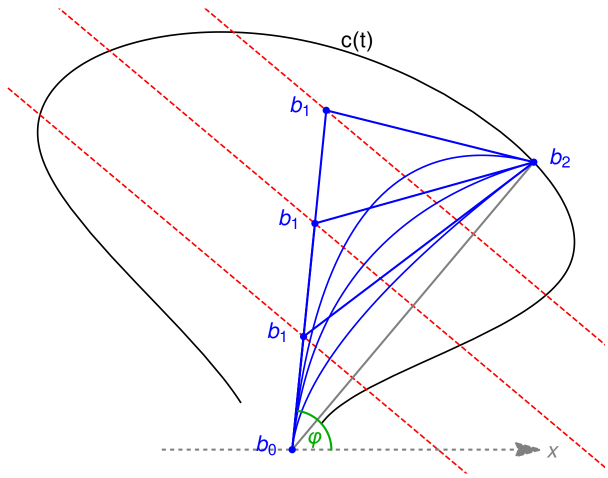


Figure 1: Parabolic arcs obtained for three different choices $\ell = \frac{1}{4}, \frac{1}{2}, \frac{3}{4}$ of the shape parameter. For any choice of the $\ell$, the control point $\mathbf{b}_1(t)$ is located on one of the red dashed lines, which are perpendicular to the line spanned by $\mathbf{b}_0$ and $\mathbf{b}_2$ (gray).

We choose the first control point at the center, the second one on the line with angle $\varphi(t)$, and the last one on the boundary $\mathbf{c}(t)$ itself:

$$\mathbf{b}_0(t) = \begin{pmatrix} 0 \\ 0 \end{pmatrix}, \tag{4}$$

$$\mathbf{b}_1(t) = \ell \frac{x(t)^2 + y(t)^2}{(x(t)\cos\varphi(t) + y(t)\sin\varphi(t))} \begin{pmatrix} \cos\varphi(t) \\ \sin\varphi(t) \end{pmatrix}, \tag{5}$$

$$\mathbf{b}_2(t) = \begin{pmatrix} x(t) \\ y(t) \end{pmatrix}. \tag{6}$$

The location of the middle point depends on the *shape parameter* $\ell$. Except for the last section of the paper, we will only consider parameterizations with a *constant* value of that parameter. In particular, we get *symmetric* arcs if $\ell = \frac{1}{2}$. We only consider values $\ell \in (0,1)$, see Figure 1.

For a given value of the shape parameter $\ell$, the parameterization with parabolic parameter lines is obtained by specifying the function $\varphi(t)$. We will call it the *design function*, since it controls the shape of the parameter lines of the parabolic arcs. The angle $\varphi(t)$ specifies the tangent direction

$$\left(\frac{\partial}{\partial s}\mathbf{p}\right)(0,t) = \frac{2\ell(x(t)^2 + y(t)^2)}{x(t)\cos\varphi(t) + y(t)\sin\varphi(t)} \begin{pmatrix} \cos\varphi(t) \\ \sin\varphi(t) \end{pmatrix}$$

of the parabolic arcs at the center. Now we introduce the central notion of this paper:

**Definition 1.** The polar parameterization (1), which is defined by the 1-periodic boundary curve $\mathbf{c}(t)$, the 1-quasiperiodic function $\varphi(t)$ with shift $2\pi$ satisfying (3) and the shape parameter $0 < \ell < 1$, is called a *polar parameterization with parabolic parameter lines* if it is regular for all $(s,t) \in (0,1] \times \mathbb{R}$.

The injectivity of polar parameterizations is discussed in the appendix. While the polar parameterizations (1) with control points (4)-(6) do not possess a tensor-product structure in general, they may serve as starting point when constructing polar tensor-product parameterizations by a fitting procedure.

*Example* (Dumbbell). We consider the 1-periodic, cubic spline curve $\mathbf{c}(t)$ with uniform knots and control points

$$\begin{pmatrix} -30 \\ 10 \end{pmatrix}, \begin{pmatrix} -25 \\ 30 \end{pmatrix}, \begin{pmatrix} -45 \\ 30 \end{pmatrix}, \begin{pmatrix} -50 \\ 0 \end{pmatrix}, \begin{pmatrix} -45 \\ -30 \end{pmatrix}, \begin{pmatrix} -25 \\ -30 \end{pmatrix}, \begin{pmatrix} -30 \\ -10 \end{pmatrix}, \begin{pmatrix} 0 \\ -5 \end{pmatrix},$$
$$\begin{pmatrix} 30 \\ -10 \end{pmatrix}, \begin{pmatrix} 25 \\ -30 \end{pmatrix}, \begin{pmatrix} 45 \\ -30 \end{pmatrix}, \begin{pmatrix} 50 \\ 0 \end{pmatrix}, \begin{pmatrix} 45 \\ 30 \end{pmatrix}, \begin{pmatrix} 25 \\ 30 \end{pmatrix}, \begin{pmatrix} 30 \\ 10 \end{pmatrix}, \begin{pmatrix} 0 \\ 5 \end{pmatrix},$$

see Fig. 2, left. The associated domain is neither star shaped nor does it possess an arc fibration. However, the domain admits a polar parameterization with parabolic parameter lines for various values of the shape parameter $\ell$. The choice of this parameter also influences the shape of the parameter lines $s$ = constant, which are shown in blue. A shortened (but still not star-shaped) version of the shape (right) admits both an arc fibration and a a polar parameterization with parabolic parameter lines, which are quite similar. $\Diamond$

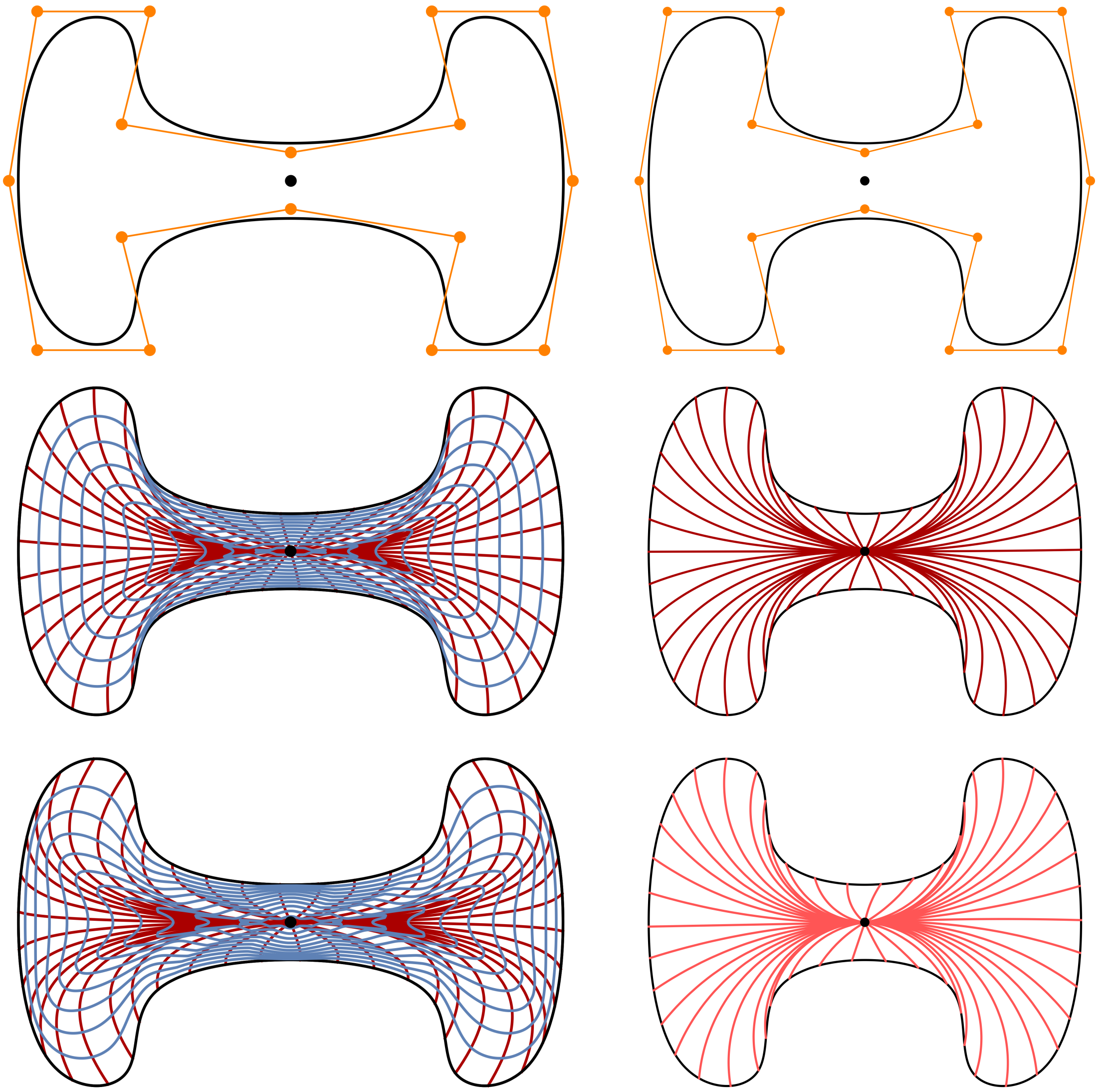

Figure 2: Dumbbell example: A planar domain (left column) that does not admit an arc fibration and an associated parameterization with parabolic parameter lines for $\ell = \frac{6}{10}$ (center) and for $\ell = \frac{9}{10}$ (bottom). Here we show both families of parameter lines. A slightly shorter version of the shape (right column) admits an arc fibration (bottom), which is fairly similar to the corresponding parameterization with parabolic parameter lines for $\ell = \frac{6}{10}$ (center).

## 3. Regularity conditions

We investigate conditions that guarantee the regularity of the parameterization by parabolas. The partial derivatives of the polar parameterization take the values

$$\frac{\partial \mathbf{p}}{\partial s}(s,t) = 2(1-2s)\mathbf{b}_1(t) + 2s\mathbf{b}_2(t) \quad \text{and} \quad \frac{\partial \mathbf{p}}{\partial t}(s,t) = 2s(1-s)\mathbf{b}_1'(t) + s^2\mathbf{b}_2'(t),$$

with

$$\begin{aligned}
\mathbf{b}_1'(t) = \ell\Bigg(&\bigg(\frac{2(x(t)x'(t)+y(t)y'(t))(x(t)\cos\varphi(t)+y(t)\sin\varphi(t))}{(x(t)\cos\varphi(t)+y(t)\sin\varphi(t))^2}\\
&-\frac{(x(t)^2+y(t)^2)(\cos\varphi(t)(x'(t)+y(t)\varphi'(t))+\sin\varphi(t)(y'(t)-x(t)\varphi'(t)))}{(x(t)\cos\varphi(t)+y(t)\sin\varphi(t))^2}\bigg)\begin{pmatrix}\cos\varphi(t)\\ \sin\varphi(t)\end{pmatrix}\\
&+\frac{(x(t)^2+y(t)^2)\varphi'(t)}{x(t)\cos\varphi(t)+y(t)\sin\varphi(t)}\begin{pmatrix}-\sin\varphi(t)\\ \cos\varphi(t)\end{pmatrix}\Bigg) \quad \text{and}\\
\mathbf{b}_2'(t) = &\begin{pmatrix}x'(t)\\ y'(t)\end{pmatrix} .
\end{aligned}$$

The Jacobian determinant of (1) evaluates to

$$J(s,t) = \frac{s}{(x(t)\cos\varphi(t)+y(t)\sin\varphi(t))^2}((1-s)^2c_0(t)+2s(1-s)c_1(t)+s^2c_2(t)) , \tag{7}$$

where the Bernstein-Bézier-coefficients of the quadratic polynomial in $s$ take the form

$$c_0(t) = 4\ell^2(x(t)^2+y(t)^2)^2\varphi'(t) , \tag{8}$$

$$c_1(t) = 2\ell(1-\ell)(x(t)^2+y(t)^2)^2\varphi'(t) + \underbrace{\frac{1}{2}\ell g(t)}_{=f(t,\varphi(t))} , \tag{9}$$

$$\begin{aligned}
c_2(t) =& 2\big(x(t)\cos\varphi(t)+y(t)\sin\varphi(t)\big)\\
&\Big(\cos\varphi(t)\big(y'(t)\big((1-\ell)x(t)^2-\ell y(t)^2\big)-x'(t)x(t)y(t)\big)\\
&+\sin\varphi(t)\big(x'(t)(\ell x(t)^2-(1-\ell)y(t)^2)+y'(t)x(t)y(t)\big)\Big) ,
\end{aligned} \tag{10}$$

with

$$\begin{aligned}
g(t) =& \big((x(t)^3-7x(t)y(t)^2)x'(t)+(7x(t)^2y(t)-y(t)^3)y'(t)\big)\sin 2\varphi(t)\\
&+\big((3y(t)^3-5x(t)^2y(t))x'(t)+(3x(t)^3-5x(t)y(t)^2)y'(t)\big)\cos 2\varphi(t)\\
&-(x(t)^2+y(t)^2)(x(t)y'(t)-y(t)x'(t)) .
\end{aligned}$$

Clearly the first factor of the Jacobian determinant in (7) is positive and we do not have to consider it, so we will focus on the second factor, which is the quadratic polynomial in $s$.

First the regularity of the parameterization along the domain boundary will be analyzed, i.e. for $s = 1$. This leads us to analyze the third coefficient $c_2(t)$, since

$$J(1,t) = \frac{1}{(x(t)\cos\varphi(t)+y(t)\sin\varphi(t))^2}c_2(t) .$$

Recall from (2) that the function $\alpha(t)$ represents the angle of the boundary points $\mathbf{c}(t)$. We use it to represent the angle of the tangent vectors $\mathbf{c}'(t)$ as $\alpha(t)+\beta(t)$ with another smooth function

$$\beta(t) \in \arg(x'(t)+iy'(t)) - \alpha(t) .$$

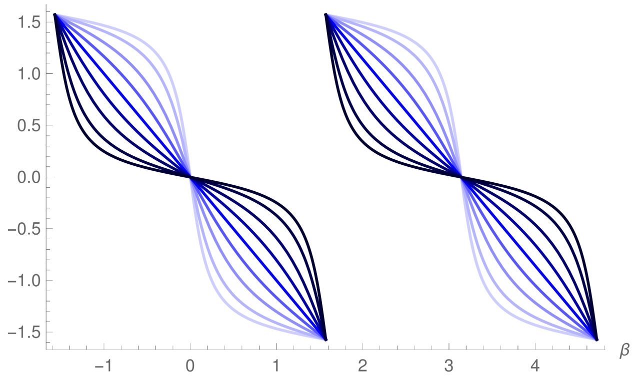


Figure 3: Graphs of the auxiliary function $\delta_\ell(\beta)$ with domain $(-\frac{\pi}{2}, \frac{\pi}{2}) \cup (\frac{\pi}{2}, \frac{3\pi}{2})$ and range $(-\frac{\pi}{2}, \frac{\pi}{2})$.

With the help of these two angles, we rewrite the Jacobian determinant as

$$J(1,t) = 2\,\|\mathbf{c}(t)\|\,\|\mathbf{c}'(t)\|\,\big((1-\ell)\sin\beta(t) + \ell\tan(\varphi(t)-\alpha(t))\cos\beta(t)\big)\ .$$

More precisely, this formula can be derived by using the identities

$$x(t) = \|\mathbf{c}(t)\|\cos\alpha(t)\ ,\ y(t) = \|\mathbf{c}(t)\|\sin\alpha(t)\ ,\ x'(t) = \|\mathbf{c}'(t)\|\cos(\alpha(t)+\beta(t))\ ,\ y'(t) = \|\mathbf{c}'(t)\|\sin(\alpha(t)+\beta(t))\ .$$

First we note that the Jacobian determinant is negative for all choices of $\varphi(t)$ if $\beta(t) = -\frac{\pi}{2} + 2k\pi$ for some $k \in \mathbb{Z}$. Consequently, no polar parameterization with parabolic parameter lines exists in this case. Thus, taking the smoothness of $\beta(t)$ into account, we may assume that

$$\beta(t) \in \left(-\frac{\pi}{2}, \frac{3\pi}{2}\right)$$

for all $t \in \mathbb{R}$. Boundary curves that satisfy this assumption will be said to be *admissible.*

Second, a short computation confirms that $J(1,t) = 0$ if and only if $\beta(t) \neq \frac{\pi}{2}$ and

$$\varphi(t) = \alpha(t) + \delta_\ell(\beta(t))$$

with the auxiliary function

$$\delta_\ell(\beta) = -\arctan\left(\frac{1-\ell}{\ell}\tan\beta\right) \quad \text{for } \beta \in \left(-\tfrac{\pi}{2}, \tfrac{3\pi}{2}\right) \setminus \left\{\tfrac{\pi}{2}\right\}.$$

Figure 3 visualizes this function for different values of the shape parameter $\ell$.

**Lemma 2.** *The Jacobian determinant $J(1,t)$ is positive if and only if the design function satisfies*

$$\varphi_{\min}(t) < \varphi(t) < \varphi_{\max}(t)$$

*with*

$$\varphi_{\min}(t) = \alpha(t) + \begin{cases} \delta_\ell(\beta(t)) & \textit{if } \beta(t) \in (-\frac{\pi}{2}, \frac{\pi}{2}) \\ -\frac{\pi}{2} & \textit{if } \beta(t) \in [\frac{\pi}{2}, \frac{3\pi}{2}) \end{cases}$$

*and*

$$\varphi_{\max}(t) = \alpha(t) + \begin{cases} \frac{\pi}{2} & \textit{if } \beta(t) \in (\frac{-\pi}{2}, \frac{\pi}{2}] \\ \delta_\ell(\beta(t)) & \textit{if } \beta(t) \in (\frac{\pi}{2}, \frac{3\pi}{2}) \end{cases}\ .$$

*Proof.* It is easy to see that at most one root of $J(1,t)$ needs to be taken into account, since the design function $\varphi(t)$ satisfies (3) and the values of $\delta_\ell$ vary in $(-\frac{\pi}{2}, \frac{\pi}{2})$. $\square$

Clearly, the criterion formulated in Lemma 2 is necessary for the regularity of the parameterization. Another necessary condition[2] is given by

$$\varphi'(t) \geq 0 \ , \tag{11}$$

since this implies $c_0(t) \geq 0$, cf. (8). We will now add another inequality to ensure the regularity for the entire polar parameterization.

We focus on the second term in (9), since the first term is already guaranteed to be non-negative by (11). First we note that the last term in the expression for $c_1(t)$, which has been defined in (9), can be rewritten as $\frac{1}{2}\ell g(t) = f(t, \varphi(t))$ with the function

$$f(t,\varphi) = A(t)\sin(2\varphi + \operatorname{Arg} B(t)) + C(t) \ , \tag{12}$$

where the three quantities $A(t), B(t), C(t)$ are defined as

$$\begin{aligned}
A(t) =& \frac{1}{2}\ell(x(t)^2 + y(t)^2)\sqrt{(x(t)x'(t) + y(t)y'(t))^2 + 9(x(t)y'(t) - y(t)x'(t))^2} \ , \\
B(t) =& (x(t)^3 - 7x(t)y(t)^2)x'(t) + (7x(t)^2y(t) - y(t)^3)y'(t) \\
& + i\big((3y(t)^3 - 5x(t)^2y(t))x'(t) + (3x(t)^3 - 5x(t)y(t)^2)y'(t)\big) \quad \text{and} \\
C(t) =& -\frac{1}{2}\ell(x(t)^2 + y(t)^2)(x(t)y'(t) - y(t)x'(t)) \ .
\end{aligned}$$

We select the two auxiliary functions $\gamma_{\min}(t)$ and $\gamma_{\max}(t)$, which are 1-quasiperiodic with shift $2\pi$, continuous, and satisfy

$$\gamma_{\min}(t) \in \frac{1}{2}\arg(\bar{B}(t)\bar{Z}(t)) \quad \text{and} \quad \gamma_{\max}(t) = \gamma_{\min}(t) + \operatorname{Arg}(Z(t)) + \frac{\pi}{2} \tag{13}$$

for all $t \in \mathbb{R}$, where

$$Z(t) = \sqrt{1 - \left(\frac{C(t)}{A(t)}\right)^2} + i\frac{C(t)}{A(t)} \ .$$

Note that the choice of these two functions is not unique, since any integer multiple of $\pi$ may be added to them.

A short computation confirms that the absolute value of $C(t)/A(t)$ cannot exceed $\frac{1}{3}$. Therefore, the argument of the complex number $Z(t)$ lies in $\left(-\arcsin\frac{1}{3}, \arcsin\frac{1}{3}\right)$, and thus the difference satisfies

$$\gamma_{\max}(t) - \gamma_{\min}(t) \in \left(\frac{\pi}{2} - \arcsin\frac{1}{3}, \frac{\pi}{2} + \arcsin\frac{1}{3}\right) \subset \left(\frac{6}{5}, 2\right) \tag{14}$$

for all $t \in \mathbb{R}$.

We have the following result:

**Lemma 3.** *The term $g(t)$ is positive, if and only if there exists an integer $k$ such that the two inequalities*

$$\gamma_{\min}(t) < \varphi(t) + k\pi < \gamma_{\max}(t)$$

*are satisfied for all $t \in \mathbb{R}$.*

[2] Though $\varphi(t)$ was required to be strictly increasing by Jüttler et al. (2019), the weaker condition is in fact sufficient for regularity of the parameterization in $(0,1] \times [0,1]$.

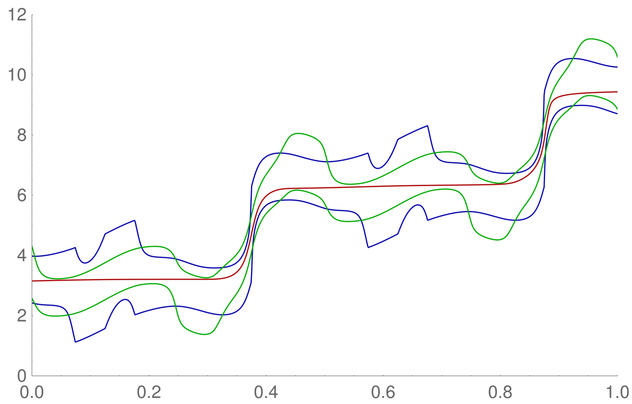


Figure 4: Graphs of the upper and lower bounds $\varphi_{\min}(t)$ and $\varphi_{\max}(t)$ (blue) and $\gamma_{\min}(t)$ and $\gamma_{\max}(t)$ (green). The design function $\varphi(t)$ is shown in red.

*Proof.* For any value of the parameter $t$, we consider the $\pi$-periodic function $f(t,\cdot)$, which is a shifted, scaled and translated copy of $\sin(2\cdot)$. A short computation confirms that its roots are given by $\gamma_{\min}(t)+\pi\mathbb{Z}$ and $\gamma_{\max}(t)+\pi\mathbb{Z}$. The derivatives of this function (hence the partial derivatives of $f$ with respect to its second argument) at these roots evaluate to

$$\frac{\partial f(t,\varphi)}{\partial\varphi}\Big|_{\varphi=\gamma_{\min}(t)} = +2A(t)\sqrt{1-\frac{C(t)^2}{A(t)^2}} \quad \text{and} \quad \frac{\partial f(t,\varphi)}{\partial\varphi}\Big|_{\varphi=\gamma_{\max}(t)} = -2A(t)\sqrt{1-\frac{C(t)^2}{A(t)^2}} \ ,$$

hence they are guaranteed to be positive at $\gamma_{\min}(t)$ and negative at $\gamma_{\max}(t)$. □

Based on these results we formulate a sufficient condition for the regularity of parameterizations by parabolic arcs:

**Theorem 4.** *The polar parameterization $\mathbf{p}(s,t)$ has parabolic parameter lines if there exists an integer $k$ such that the design function $\varphi(t)$ satisfies*

$(i)$ $\varphi'(t) \geq 0$ ,

$(ii)$ $\varphi_{\min}(t) < \varphi(t) < \varphi_{\max}(t)$ *and*

$(iii)$ $\gamma_{\min}(t) < \varphi(t) + k\pi < \gamma_{\max}(t)$

*for all $t \in \mathbb{R}$.*

*Proof.* Using Lemma 2 and Lemma 3, we conclude that the Jacobian determinant of the parameterization is positive for all $(s,t) \in (0,1] \times \mathbb{R}$, provided that the three conditions $(i)-(iii)$ are fulfilled. □

*Example* (Dumbbell, continued). Once more, we consider the dumbbell-shaped domain of the Dumbbell Example and the shape parameter $\ell = \frac{9}{10}$. With the aim of obtaining a parameterization with parabolic parameter lines, the design function $\varphi(t)$ is chosen such that it fulfills the assumptions of Theorem 4. It is a smooth, increasing quasiperiodic function with period 1 and constant $2\pi$, satisfying $\varphi_{\min}(t) < \varphi(t) < \varphi_{\max}(t)$ and $\gamma_{\min}(t) < \varphi(t) < \gamma_{\max}(t)$. A cubic spline defined by 14 polynomial segments in $[0,1]$ and manually chosen spline coefficients has been designed that meet these conditions. The graphs of the various upper and lower bounds and of the design function itself are shown in Figure 4. Figure 2 visualizes the corresponding parameterization with parabolic parameter lines on the left-hand side, bottom. ◊

## 4. Computation

We present an algorithm that decides if there exists a function $\varphi(t)$, which fulfills the three conditions of Theorem 4 for a given planar curve $\mathbf{c}(t)$ with respect to a certain center point and a specific choice of the shape parameter $\ell$. Further the algorithm should generate, if possible, a valid function $\varphi(t)$.

The 1-quasiperiodic functions $\varphi_{\min}(t)$, $\varphi_{\max}(t)$, $\gamma_{\min}(t)$ and $\gamma_{\max}(t)$, define the $\varphi$- and the $\gamma$-channel

$$\begin{aligned} C_\varphi &= \left\{(\xi,\eta) \in \mathbb{R}^2 : \varphi_{\min}(\xi) < \eta < \varphi_{\max}(\xi)\right\} \\ C_\gamma^k &= \left\{(\xi,\eta) \in \mathbb{R}^2 : \gamma_{\min}(\xi) < \eta < \gamma_{\max}(\xi)\right\} + k\pi \ , \quad k \in \mathbb{Z} \ , \\ C_\gamma &= \bigcup_{k\in\mathbb{Z}} C_\gamma^k \ . \end{aligned}$$

Since the difference of $\gamma_{\min}(t)$ and $\gamma_{\max}(t)$ doesn't exceed 2 (see (14)), the $\gamma$-channel consists of disjoint branches $C_\gamma^k$, one for each integer k, since

$$\gamma_{\max}(t) + k\pi < \gamma_{\min}(t) + (k+1)\pi \quad \forall k \in \mathbb{Z} \forall t \in \mathbb{R} \ .$$

An increasing, 1-quasiperiodic function $\varphi(t)$ fulfills the conditions of Theorem 4, if the graph is contained in $C_\varphi \cap C_\gamma$. We exploit the monotonicity and define the reduced channels

$$\begin{aligned} \hat{C}_\varphi &= \left\{(\xi,\eta) \in \mathbb{R}^2 : \hat{\varphi}_{\min}(\xi) < \eta < \hat{\varphi}_{\max}(\xi)\right\} \quad \text{and} \\ \hat{C}_\gamma^k &= \left\{(\xi,\eta) \in \mathbb{R}^2 : \hat{\gamma}_{\min}(\xi) < \eta < \hat{\gamma}_{\max}(\xi)\right\} + k\pi \ , \\ \hat{C}_\gamma &= \bigcup_{k\in\mathbb{Z}} \hat{C}_\gamma^k \ . \end{aligned}$$

with the help of the modified boundary functions

$$\begin{aligned} \hat{\varphi}_{\min}(t) &= \max_{\tau\le t} \varphi_{\min}(\tau) \quad \text{and} \quad \hat{\varphi}_{\max}(t) = \min_{\tau\ge t} \varphi_{\max}(\tau) \ , \\ \hat{\gamma}_{\min}(t) &= \max_{\tau\le t} \gamma_{\min}(\tau) \quad \text{and} \quad \hat{\gamma}_{\max}(t) = \min_{\tau\ge t} \gamma_{\max}(\tau) \ . \end{aligned}$$

Clearly, it is only possible to find a suitable design function $\varphi(t)$ with its graph contained in the intersection of the reduced channels, if at least one of the intersections

$$\hat{C}^k = \hat{C}_\varphi \cap \hat{C}_\gamma^k \tag{15}$$

is connected. The sufficient conditions

$$[\hat{\gamma}_{\min}(0), \hat{\gamma}_{\max}(0)] + k\pi \cap [\hat{\varphi}_{\min}(0), \hat{\varphi}_{\max}(0)] \neq \emptyset \ . \tag{16}$$

characterize the at most two instances of $k$ that may lead to connected intersection. The associated intersection (15) is then connected if

$$\forall t : \quad \max\{\hat{\varphi}_{\min}(t), \hat{\gamma}_{\min}(t) + k\pi\} < \min\{\hat{\varphi}_{\max}(t), \hat{\gamma}_{\max}(t) + k\pi\} \tag{17}$$

holds. Consequently, we may find a design function $\varphi(t)$ that fulfills the conditions of Theorem 4 if the conditions (17) are fulfilled for some choice of $k$, and it suffices to analyze the two instances of $k$ that satisfy (16). In this situation, we generate $\varphi(t)$ as a monotonic spline approximation of the center curve

$$\psi(t) = \frac{1}{2}\big(\min\{\hat{\varphi}_{\max}(t), \hat{\gamma}_{\max}(t) + k\pi\} + \max\{\hat{\varphi}_{\min}(t), \hat{\gamma}_{\min}(t) + k\pi\}\big) \ ,$$

which is 1-quasiperiodic with shift $2\pi$. One particularly simple way to find such an approximation

$$\varphi(t) = \sum_{j\in\mathbb{Z}} N_j^p(t)\psi(\xi_j) \ . \tag{18}$$

is to use B-splines of some degree $p \geq 2$ with respect to the bi-infinite knots $h\mathbb{Z}$, where the control points are constructed by sampling the center curve at the (also uniformly spaced) Greville abscissae $\xi_j$. It is contained within $\hat{C}^k$ for sufficiently dense knots, and it inherits the monotonicity of the center curve due to the shape-preserving properties of B-splines.

We summarize these observations in an algorithm, which takes as input the boundary curve $\mathbf{c}(t)$ and the shape parameter $\ell$ and decides if the sufficient conditions of Theorem 4 can be satisfied. If possible, it chooses a design function $\varphi(t)$ and computes the parameterization with parabolic parameter lines.

1. First, it has to be checked if the curve $\mathbf{c}(t)$ is admissible, i.e. if $\beta(t) \in (-\frac{\pi}{2}, \frac{3\pi}{2})$ holds for all $t \in \mathbb{R}$. The computation is aborted if the curve is not admissible. The domain does not possess a parameterization with parabolic parameter lines.
2. Compute the reduced $\gamma$-channel $\hat{C}^0_\gamma$ and check if it is connected, cf. Eq. (17). The computation is aborted if the channel is not connected. With this choice of the center, the sufficient condition of the Theorem cannot be fulfilled.
3. Generate the reduced $\varphi$-channel $\hat{C}_\varphi$ and check if it is connected. The computation is aborted if the channel is not connected. With this choice of the shape parameter $\ell$ and/or the center, the sufficient condition of the Theorem cannot be fulfilled.
4. Find all integers $k$ that satisfy (16) and check if at least one of the associated channels $\hat{C}^k$ is connected. The computation is aborted otherwise. With this choice of the shape parameter $\ell$ and/or the center, the sufficient condition of the Theorem cannot be fulfilled.
5. Choose a smooth, increasing, 1-quasiperiodic function $\varphi(t)$ with shift $2\pi$ such that the graph of the function is contained in (one of) the connected channel(s) $\hat{C}^k$. For example, one may choose the spline approximation defined in Eq. (18).
6. Generate and return the polar parameterization with parabolic parameter lines for the domain, see Eq. (1).

In our current implementation, we simply discretize the channels numerically in order to check their connectivity. More advanced methods could be investigated for special classes of boundary curves (similar to the case of arc fibrations (Weiß and Jüttler, 2019; Weiß, 2019), where the computations become particularly elegant for domains with arc spline boundaries), but this is beyond the scope of the present paper. If the computation is aborted, the user may modify the input (the shape parameter $\ell$ and the center points) in order to obtain a parameterization with parabolic parameter lines. While it is always possible (but also expensive) to employ a sampling-based approach, we will outline some preliminary ideas regarding the choice of the center in the conclusion.

## 5. Examples

We apply the algorithm to several domains:

*Example* (Fish). We consider a fish-shaped domain defined by a uniform cubic spline curve with 12 control points, see Figure 5(a), the center shown in the figure and the shape parameter $\ell = \frac{6}{10}$. For the first choice of the center, the algorithm is aborted after the second step, since the reduced $\gamma$-channel (boundaries shown in green in (b)) is not connected. When considering another center point (shown in (c)), however, the algorithm succeeds to generate a valid parameterization with parabolic parameter lines, since a connected $\hat{C}^k$ is found. In Figure 5(d) the design function $\varphi(t)$ is plotted in red. $\Diamond$

*Example* (Clover). We examine a planar domain in the shape of a four-leaf clover, defined by a uniform cubic spline curve with 32 control points, and the center shown in Figure 6(left). We analyze three different values $\frac{1}{10}$, $\frac{3}{10}$, $\frac{8}{10}$ of the shape parameter $\ell$. For the first choice, the algorithm is aborted after the third step, since the reduced $\varphi$-channel is not connected, see Figure 6(right). For the second and the third choice, the algorithm succeeds and generates a valid parameterization with parabolic parameter lines, see Figure 7. By comparing the two parameterizations we can see how the parameter $\ell$ influences the shape of the parameter line. While for $\ell = \frac{3}{10}$ the parameter lines are close to straight lines, in the case of $\ell = \frac{8}{10}$ the lines are much more curved. $\Diamond$

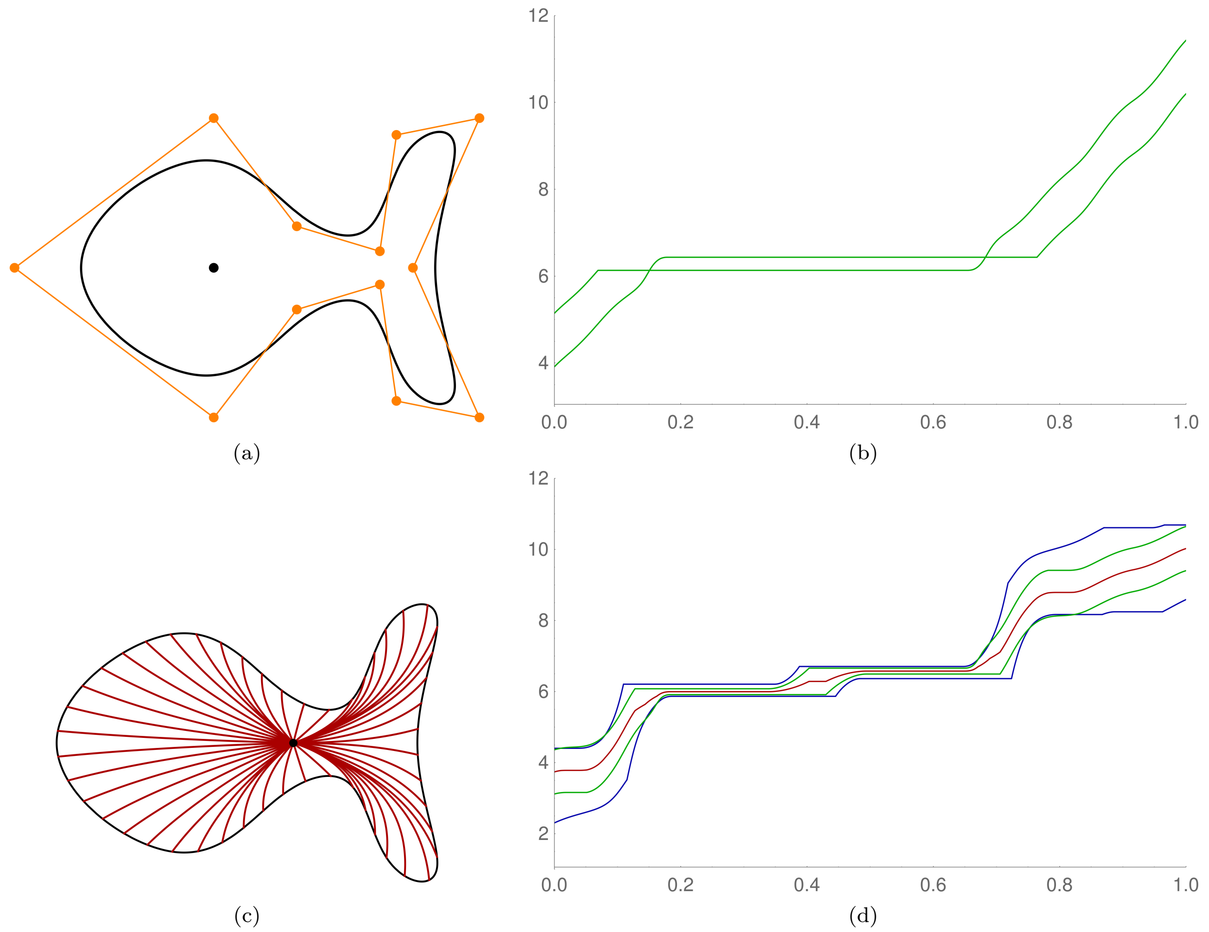


Figure 5: Fish Example: Generating a parameterization with parabolic parameter lines of a fish-shaped domain (left column). The boundaries of the reduced $\gamma$- and $\varphi$-channels are shown in green and blue, respectively (right column).

*Example* (Tamper). We consider a tamper-shaped planar domain defined by a uniform cubic spline with 16 control points and the center shown in Figure 8(a). The algorithm aborts for the first choice of the shape parameter $\ell = \frac{8}{10}$, stating that the channel $\hat{C}^k$ is not connected. In Figure 8 (b) we see that the individual reduced $\gamma$- and $\varphi$-channels are connected but the intersection is not. For the second choice $\ell = \frac{6}{10}$ of the shape parameter, the algorithm succeeds. Figures 8(c,d) visualize the parameterizations and the boundaries of the corresponding reduced channels. $\Diamond$

*Example* (Pi). The simple planar domain in the shape of the Greek letter $\pi$ is defined by a uniform cubic spline with 16 control points, see Fig. 9. The reduced $\varphi$-channel is connected for all values of $\ell \in [\frac{1}{10}, \frac{9}{10}]$. Connected intersections $\hat{C}^k$ are obtained for a much smaller range, which includes $\ell \in \{\frac{5}{10}, \frac{6}{10}, \frac{7}{10}\}$. The algorithm generates a valid parameterization with parabolic parameter lines, e.g., for $\ell = \frac{6}{10}$, which is also shown in Fig. 9. $\Diamond$

## 6. Extension to non-constant shape parameter

We present the extension to a non-constant shape parameter $\ell(t)$. We restrict ourselves to shape parameter functions with values $\ell(t) \in (0, 1)$ for all $t \in \mathbb{R}$. Moreover, these functions need to be $C^1$-smooth and 1-periodic, i.e.,

$$\ell(t+1) = \ell(t) \ .$$

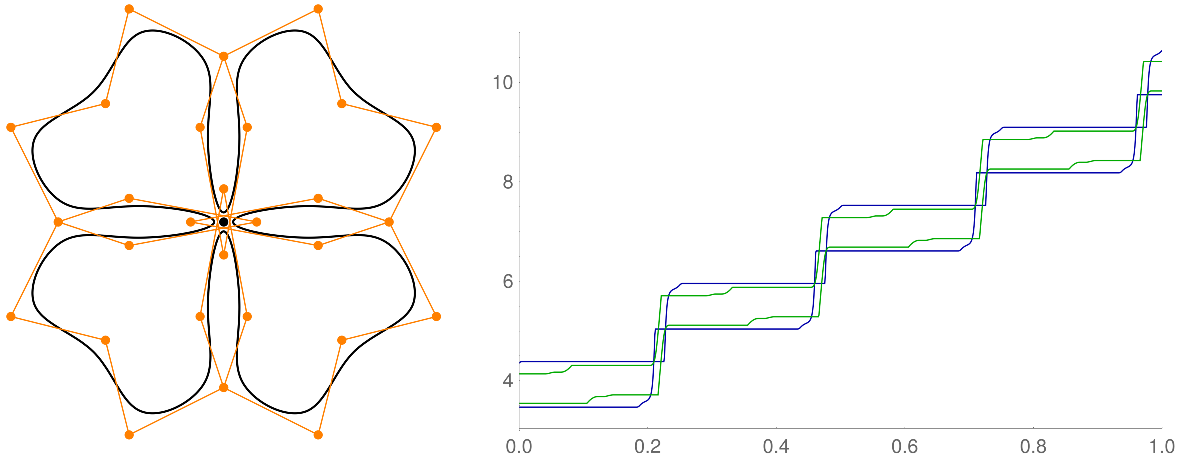


Figure 6: Clover Example: When trying to generate a parameterization with parabolic parameter lines of a clover-shaped domain (left) for $\ell = \frac{1}{10}$, the algorithm aborts and states that the reduced $\varphi$-channel (blue) is not connected (right).

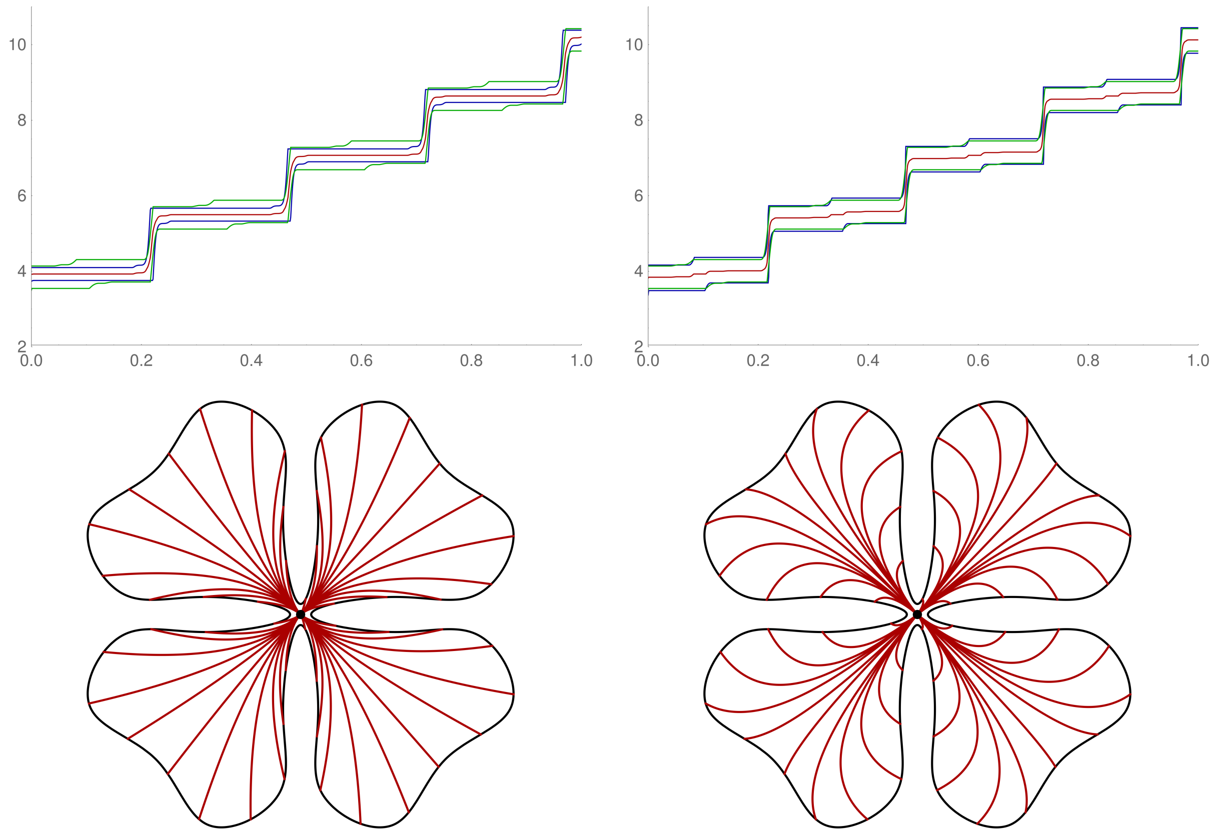


Figure 7: Clover Example: Generating a parameterization with parabolic parameter lines for two different choice of the shape parameter $\ell = \frac{3}{10}$ in the left column and $\ell = \frac{8}{10}$ in the right column. Top: The boundaries of the reduced $\gamma$- and $\varphi$-channels are visualized in green and blue, respectively. Bottom: The parameterizations with parabolic parameter lines are plotted.

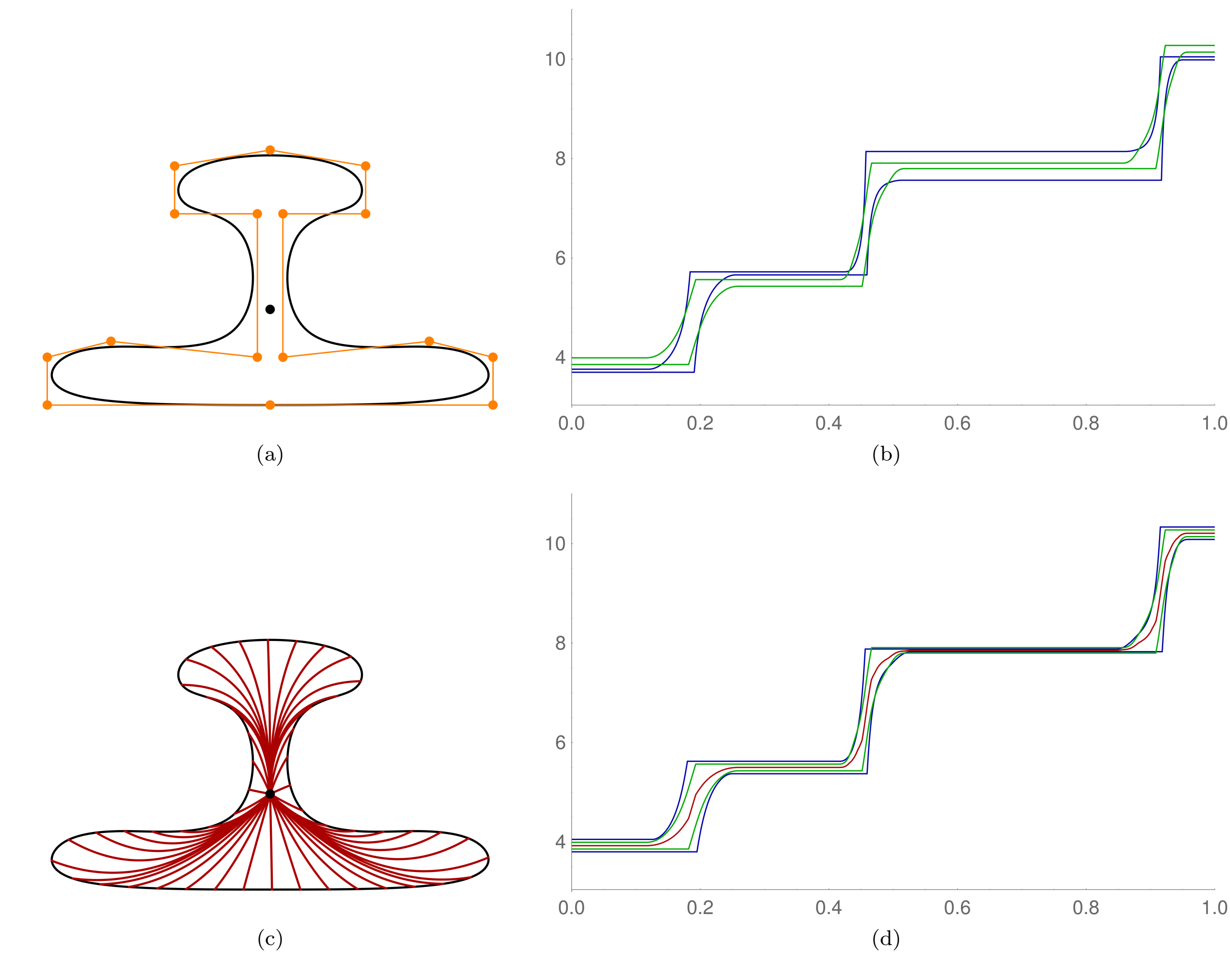


Figure 8: Tamper Example: Top: Domain (with center) and the reduced channels for $\ell = \frac{8}{10}$. Bottom: Parameterization with parabolic parameter lines and the reduced channels for $\ell = \frac{6}{10}$.

We obtain again polar parameterizations of the form (1) with $\mathbf{b}_0(t)$, $\mathbf{b}_2(t)$ defined as in (4) and (6) and with the middle control point

$$\mathbf{b}_1(t) = \ell(t)\frac{x(t)^2 + y(t)^2}{(x(t)\cos\varphi(t) + y(t)\sin\varphi(t))}\begin{pmatrix}\cos\varphi(t)\\ \sin\varphi(t)\end{pmatrix}.$$

The Jacobian determinant of this parameterization, now evaluates to

$$\bar{J}(s,t) = \frac{s}{(x(t)\cos\varphi(t) + y(t)\sin\varphi(t))^2}\left((1-s)^2 c_0(t) + 2s(1-s)\bar{c}_1(t) + s^2 c_2(t)\right),$$

where the Bernstein-Bézier-coefficients $c_0$ and $c_2$ are defined as in (8) and (10) (but with non-constant shape parameter $\ell(t)$), and the middle coefficient takes the form

$$\bar{c}_1(t) = 2\ell(t)(1-\ell(t))(x(t)^2 + y(t)^2)^2\varphi'(t) + \underbrace{\frac{1}{2}\ell(t)\bar{g}(t) + \ell'(t)\bar{h}(t)}_{=\bar{f}(t,\varphi(t))},$$

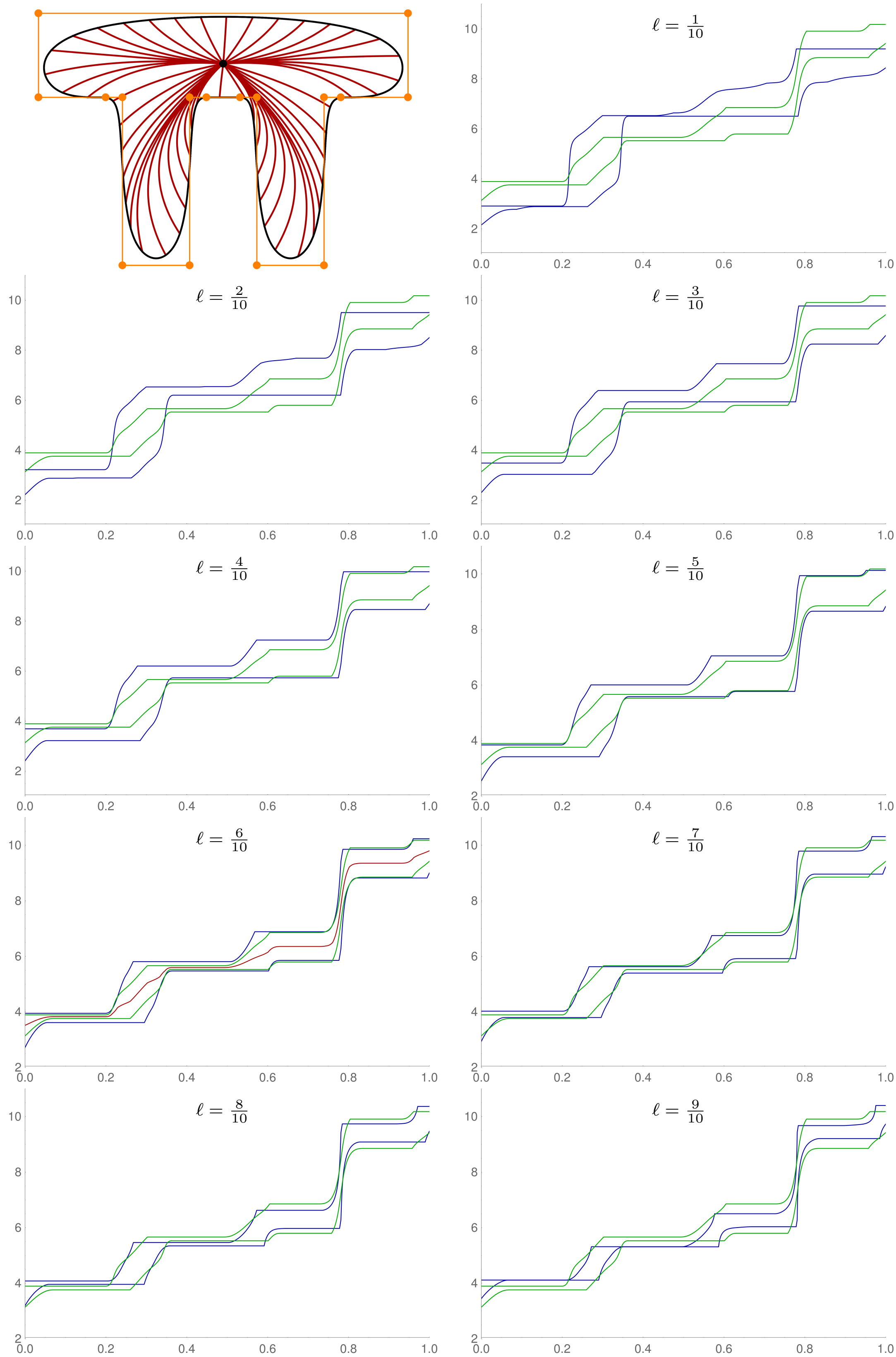


Figure 9: Pi Example: The pi-shaped planar domain with the control polygon of the boundary curve (top left) and the resulting polar parameterization, and the reduced channels for $\ell = \frac{i}{10}$ with $i = 1, \ldots, 9$ with the design function (red) for $i = 6$.

with

$$\begin{aligned}\bar{g}(t) =&((x(t)^3 - 7x(t)y(t)^2)x'(t) + (7x(t)^2y(t) - y(t)^3)y'(t)) \cos\varphi(t) \sin\varphi(t)+\\ &((y(t)^3 - x(t)^2y(t))x'(t) + (x(t)^3 - 3x(t)y(t)^2)y'(t))(\cos\varphi(t))^2+\\ &((3x(t)^2y(t) - y(t)^3)x'(t) + (x(t)y(t)^2 - x(t)^3)y'(t))(\sin\varphi(t))^2 \quad \text{and}\\ \bar{h}(t) =&(x(t)^2 + y(t)^2)((x(t)^2 - y(t)^2) \sin 2\varphi(t) - 2x(t)y(t) \cos 2\varphi(t)) \ .\end{aligned}$$

Note that the the derivative of the shape parameter appears in the formula for the second control point $\bar{c}_1(t)$. In order to derive sufficient conditions for positivity, we rewrite the last two terms as

$$\bar{f}(t, \varphi) = \bar{A}(t) \sin(2\varphi + \operatorname{Arg} \bar{B}(t)) + \bar{C}(t) \ ,$$

analogously to (12). The three coefficients $\bar{A}(t)$, $\bar{B}(t)$, $\bar{C}(t)$ take the values

$$\begin{aligned}\bar{A}(t) =&\frac{1}{2}(x(t)^2 + y(t)^2)\\ &\sqrt{\big(2\ell'(t)(x(t)^2 + y(t)^2) + \ell(t)(x(t)x'(t) + y(t)y'(t))\big)^2 + 9\ell(t)^2(x(t)y'(t) - y(t)x'(t))^2} \ ,\\ \bar{B}(t) =&\ell(t)((x(t)^3 - 7x(t)y(t)^2)x'(t) + (7x(t)^2y(t) - y(t)^3)y'(t)) + 2\ell'(t)(x(t)^4 - y(t)^4)\\ &+ i\big(\ell(t)((3y(t)^3 - 5x(t)^2y(t))x'(t) + (3x(t)^3 - 5x(t)y(t)^2)y'(t))\\ &- 4\ell'(t)x(t)y(t)(x(t)^2 + y(t)^2)\big) \quad \text{and}\\ \bar{C}(t) =& -\frac{1}{2}\ell(t)(x(t)^2 + y(t)^2)(x(t)y'(t) - y(t)x'(t)) \ .\end{aligned}$$

Again we select the two auxiliary functions $\bar{\gamma}_{\min}(t)$ and $\bar{\gamma}_{\max}(t)$, which are 1-quasiperiodic with shift $2\pi$, continuous, and satisfy (13) with the new quantities $\bar{A}(t)$, $\bar{B}(t)$ and $\bar{C}(t)$. Since the absolute value of $\bar{C}(t)/\bar{A}(t)$ is bounded by $\frac{1}{3}$, the difference of the auxiliary functions satisfies (14) for all $t \in \mathbb{R}$. Accordingly, the term

$$\frac{1}{2}\ell(t)\bar{g}(t) + \ell'(t)\bar{h}(t)$$

is positive, if and only if the conditions of Lemma 3 are satisfied.

Summing up, we may use the algorithm and the definition of the channels as before, but with the redefined boundary functions $\bar{\gamma}_{\min}(t)$ and $\bar{\gamma}_{\max}(t)$. It should be noted that the $\bar{\gamma}$-channel also depends on the choice of the shape parameter $\ell(t)$, which was not the case for a constant shape parameter.

*Example* (Big Tamper). We consider another tamper-shaped planar domain defined by a uniform cubic spline with 16 control points and the center shown in Figure 10(a). First we consider a constant value for the shape parameter but the algorithm aborts, because the reduced $\gamma$-channel is not connected, see Figure 10(b). Also when considering different locations of the center point, we did not succeed to obtain a reduced $\gamma$-channel that is connected. However, when employing the non-constant shape parameter function $\ell(t)$ shown in Figure 10(c), the algorithm succeeds and generates a valid parameterization with parabolic parameter lines. $\Diamond$

## 7. Conclusion

Polar parameterizations of planar domains with parabolic parameter lines form a potentially useful generalization of the arc fibrations that were studied by Jüttler et al. (2019). According to our experience (cf. the "Dumbbell" example), these parameterizations give similar results for shapes admitting arc fibrations, and are substantially more flexible than those. We presented sufficient conditions for the regularity and derived an algorithm for constructing such parameterizations. While the first part of the paper was devoted to the case of a constant shape parameter $\ell$, which was introduced in order to reduce the geometric complexity of the problem, the generalization to non-constant shape parameters was studied as well.

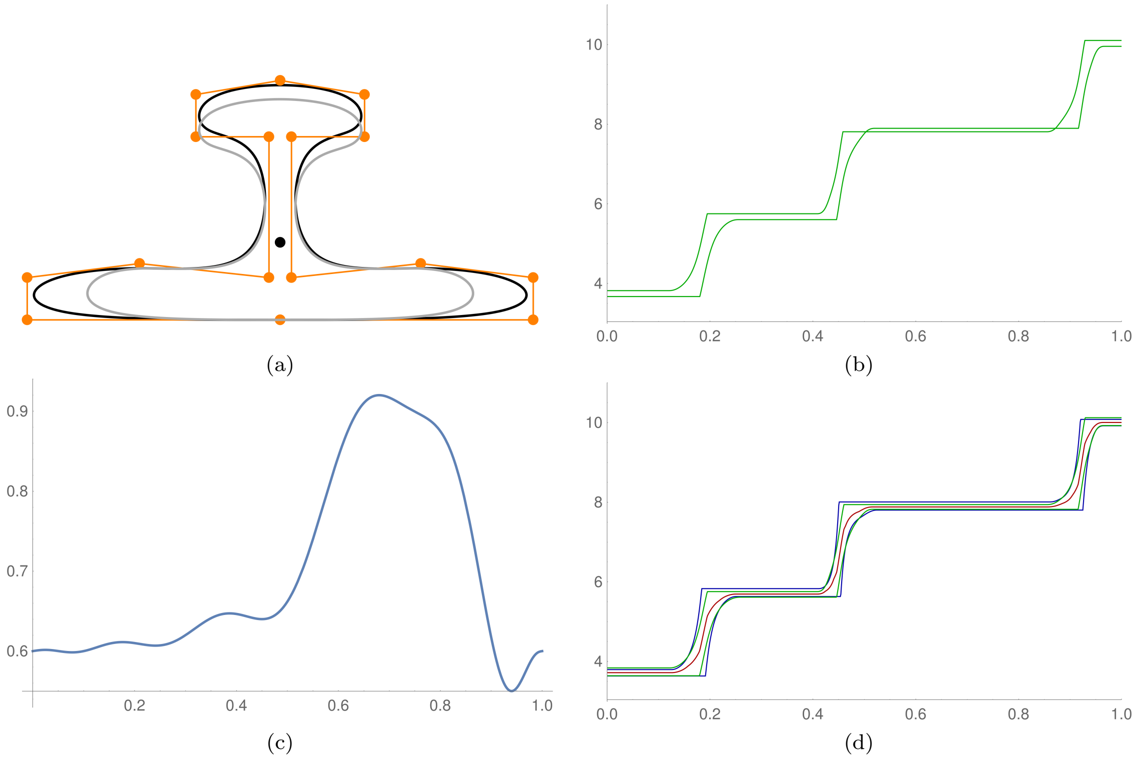

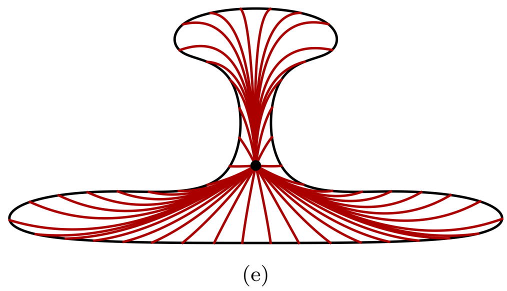

Figure 10: Big Tamper Example: We compare to the domain to the first Tamper example (a) and note that the reduced $\gamma$-channel (for a constant value of $\ell$) is disconnected (b). For a non-constant shape parameter (c), the algorithm succeeds and generates a valid parameterization with parabolic parameter lines (e), since $\hat{C}^k$ is connected (d).

Future work should be devoted to the kernel of a domain with respect to this class of polar parameterizations. More precisely, it should be interesting to analyze the set of centers that lead to regular polar parameterizations with parabolic parameter lines. Figure 11 reports some preliminary results for the dumbbell example: We sampled various locations of the center point and checked whether the resulting reduced $\gamma$-channels are connected or not. This information may be useful when choosing the center point. Besides, the construction of parameterizations that are optimal with respect to certain quality criteria could be of potential interest.

## Appendix: Injectivity of polar parameterizations

The injectivity of parameterization with non-vanishing Jacobian determinant is well understood (Kestelman, 1971). For the sake of completenes we discuss the extension to the case of polar parameterizations:

**Proposition 5.** *A polar parameterization with positive Jacobian determinant is a bijective mapping between* $(0,1]^2$ *and* $\bar{D} \setminus \{\mathbf{0}\}$.

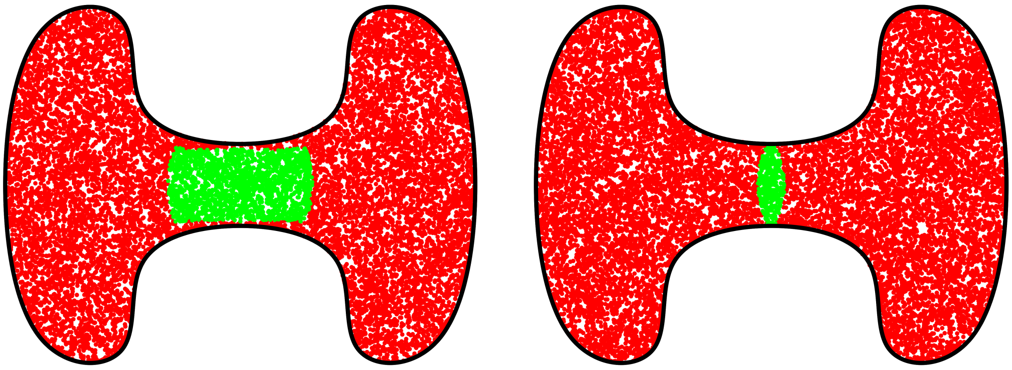

Figure 11: Dumbbell example: Center points that lead to a connected (green) and disconnected (red) reduced $\gamma$-channel (left), and that are suitable (green) and unsuitable (red) for defining an arc fibration.

*Proof.* We use Green's theorem to express the area of the domain $D$ as a boundary integral

$$|D| = \iint_D 1 \,\mathrm{d}q_1 \,\mathrm{d}q_2 = \oint_{\partial D} 0 \,\mathrm{d}q_1 + q_1 \,\mathrm{d}q_2 = \int_0^1 p_1(1,t)\partial_t p_2(1,t)\,\mathrm{d}t \ .$$

This can be extended to an integral

$$|D| = \int_0^1 p_1(s,0)\partial_s p_2(s,0)\,\mathrm{d}s + \int_0^1 p_1(1,t)\partial_t p_2(1,t)\,\mathrm{d}t + \int_1^0 p_1(s,1)\partial_s p_2(s,1)\,\mathrm{d}s + \int_1^0 p_1(0,t)\partial_t p_2(0,t)\,\mathrm{d}t$$

over the entire boundary of the unit square, since the first and the third term sum to zero (as the parameterization is 1-periodic with respect to $t$) and the fourth therm evaluates to zero (as $\mathbf{p}(0,t) = \mathbf{0}$). Another application of Green's theorem confirms

$$\begin{aligned} |D| &= \oint_{\partial[0,1]^2} p_1(s,t)\partial_s p_2(s,t)\mathrm{d}s + p_1(s,t)\partial_t p_2(s,t)\mathrm{d}t \\ &= \iint_{[0,1]^2} \partial_s p_1(s,t)\partial_t p_2(s,t) - \partial_t p_1(s,t)\partial_s p_2(s,t)\,\mathrm{d}s\,\mathrm{d}t \end{aligned}$$

After choosing an arbitrary positive integer $N$, we may split this integral into the $N^2$ sub-integrals

$$|D| = \sum_{i=1}^{N}\sum_{j=1}^{N} \iint_{C_{ij}} |J(s,t)|\,\mathrm{d}s\,\mathrm{d}t$$

with respect to the mutually disjoint cells

$$C_{ij} = (\frac{i-1}{N}, \frac{i}{N}] \times (\frac{j-1}{N}, \frac{j}{N}]$$

that cover the unit square $(0,1]^2$, where

$$J(s,t) = \partial_s p_1(s,t)\partial_t p_2(s,t) - \partial_t p_1(s,t)\partial_s p_2(s,t)$$

denotes the Jacobian determinant, which is guaranteed to be positive due to the regularity assumption. These sub-integrals are all positive and are upper bounds on the areas of the subdomains, which are obtained by restricting the parameters $(s,t)$ to the interiors $C_{ij}^\circ$ of the cells. The additivity of the area thus implies that all these subdomains are mutually disjoint.

Let us assume that the mapping $\mathbf{p}$ is not bijective. Then there exist two points satisfying $\mathbf{p}(s_1, t_1) = \mathbf{p}(s_2, t_2)$. It is easy to see that no inner point is mapped to the domain boundary, thus both points are inner points as the boundary parameterization is bijective on $(0, 1]$. The two points do not belong to the same cell if $N > 1/\max(|s_1 - s_2|, |t_1 - t_2|)$. Thus we can find an integer $N$ such that the two points are located in the interiors of two different cells. (We may consider the mapping $\mathbf{p}(s + \epsilon, t)$ for a small perturbation $\epsilon$ if $s_1 = 0$ or $s_2 = 0$.) This contradicts the previously noted result that the corresponding image subdomains are mutually disjoint. □

## Acknowledgement

Supported by the European Research Council through grant GA no. 694515 "CHANGE".

## References

Arioli, C., Shamanskiy, A., Klinkel, S., Simeon, B., 2019. Scaled boundary parametrizations in isogeometric analysis. Comp. Meth. Appl. Mech. Eng. 349, 576–594.

Avis, D., Toussaint, G., 1981. An efficient algorithm for decomposing a polygon into star-shaped polygons. Pattern Recognition 13, 396–398.

Chen, L., Simeon, B., Klinkel, S., 2016. A NURBS based Galerkin approach for the analysis of solids in boundary representation. Comp. Meth. Appl. Mech. Eng. 305, 777–805.

Dobkin, D., Souvaine, D., 1990. Computational geometry in a curved world. Algorithmica 5, 421–457.

Elber, G., Sayegh, R., Barequet, G., Martin, R., 2005. Two-dimensional visibility charts for continuous curves, in: Proc. Int. Conf. Shape Modeling and Applications, pp. 208–217.

Gondegaon, S., Voruganti, H., 2018. An efficient parametrization of planar domain for isogeometric analysis using harmonic functions. J. Braz. Soc. Mech. Sciences Engrg. 40. Article no. 493.

Joshi, S., Rao, Y., Sundar, B.R., Muthuganapathy, R., 2017. On the visibility locations for continuous curves. Comp. Graph. 66.

Jüttler, B., Maroscheck, S., Kim, M.S., Youn Hong, Q., 2019. Arc fibrations of planar domains. Comp. Aided Geom. Des. 71, 105–118.

Kestelman, H., 1971. Mappings with non-vanishing Jacobian. The American Mathematical Monthly 78, 662–663.

Lee, D., Preparata, F., 1979. An optimal algorithm for finding the kernel of a polygon. J. ACM 26, 415–421.

Lin, G., Zhang, Y., Hu, Z., Zhong, H., 2014. Scaled boundary isogeometric analysis for 2D elastostatics. Science China: Physics, Mechanics and Astronomy 57, 286–300.

Natarajan, S., Wang, J., Song, C., Birk, C., 2015. Isogeometric analysis enhanced by the scaled boundary finite element method. Comp. Meth. Appl. Mech. Eng. 283, 733–762.

O'Rourke, J., Supowit, K., 1983. Some NP-hard polygon decomposition problems. IEEE Trans. Inf. Theory 29, 181–190.

Piegl, L.A., Tiller, W., Rajab, K., 2014. It is time to drop the 'R' from NURBS. Eng. Comp. 30, 703–714.

Weiß, B., 2019. Mitered Offsets, Skeletons and Arc Fibrations of planar free-form shapes. Ph.D. thesis. Johannes Kepler University. Linz/Austria.

Weiß, B., Jüttler, B., 2019. Arc fibrations of planar domains with arc spline boundaries. Submitted for publication.